Coalescence towards exceptional contours in synthetic phononic media

2016 EPL 114 47007

(http://iopscience.iop.org/0295-5075/114/4/47007)

A Letters Journal Exploring the Frontiers of Physics

May 2016

EPL, **114** (2016) 47007
doi: 10.1209/0295-5075/114/47007

www.epljournal.org

Coalescence towards exceptional contours in synthetic phononic media

J. Christensen

Department of Photonics Engineering, Technical University of Denmark - DK-2800 Kgs. Lyngby, Denmark

received 5 April 2016; accepted in final form 30 May 2016
published online 20 June 2016

PACS 77.55.hf – ZnO
PACS 77.65.Dq – Acoustoelectric effects and surface acoustic waves (SAW) in piezoelectrics
PACS 11.30.Er – Charge conjugation, parity, time reversal, and other discrete symmetries

Abstract – Parity-time ($\mathcal{PT}$) symmetric media, also referred to as synthetic media, have been devised in many optical systems with the ground breaking potential to create non-reciprocal structures and one-way cloaks of invisibility. Here we demonstrate a feasible approach for the case of sound where gain and loss are induced via the acousto-electric effect in electrically biased piezoelectric semiconductors. We study how wave attenuation and amplification can be tuned, and when combined, can give rise to phononic $\mathcal{PT}$ synthetic media with unidirectional suppressed reflectance, a feature directly applicable to evading sonar detections.

Introduction. – Carefully mixing gain and loss in structured media can lead to physical systems that are invariant under time inversion and mirror reflection, in short, parity-time ($\mathcal{PT}$) symmetric. An important feature of these systems is the exceptional point that is a degeneracy intrinsically linked to non-Hermitian Hamiltonians. At that point, two complex eigenvalues coalesce in both their real and imaginary parts. The modal interference between these solutions can give rise to one-way suppression of the reflectance and power oscillations are also induced. Classical optics, but also electronics and optomechanics have shown in recent years to be versatile playgrounds to test these properties among many other effects with great potential for unidirectional light propagation and coherent perfect absorbers [1–14].

Recently, two experiments verified that $\mathcal{PT}$ symmetry can be translated to acoustic waves. The ingredients are the same, loss and gain. Loss obviously is given in nature but the gain counterpart is difficult to archive since no natural media can amplify sound waves. One of the aforementioned experiments applied one loudspeaker loaded with an absorbing circuit, and a second operated with an active electrical circuit tailored to realize the time-reversed image of the first loudspeaker [15]. The other experiment used the lossy nature of the waveguide and combined it with a feedback system [16]. These coupled units constitute a $\mathcal{PT}$-symmetric system with balanced loss and gain. In this article, we demonstrate the phononic version of $\mathcal{PT}$ symmetry in binary systems containing a gain and a loss unit. We take advantage of the acousto-electric effect in piezoelectric semiconductors such as ZnO (other materials like GaAs, GaN, InSb, etc. are also possible) and show how loss and gain can be tailored at will through electric bias. Above a certain balanced gain-loss threshold, $\mathcal{PT}$ symmetry is spontaneously broken, the system changes from entirely real-valued to complex and suppression of the acoustic reflectance in one direction is possible.

Theoretical framework. – We begin by writing the constitutive piezoelectric equations together with the equations of motion

$$\begin{aligned} T_{ij} &= c_{ijkl}S_{kl} - e_{kij}E_k, \\ D_i &= e_{ijk}S_{jk} + \varepsilon_{ij}E_j, \\ \rho\frac{\partial^2 u_i}{\partial t^2} &= \frac{\partial T_{ij}}{\partial x_j}, \end{aligned} \tag{1}$$

where T_{ij}, S_{kl}, D_i, E_j, c_{ijkl}, e_{ijkl}, ε_{ij}, ρ, and u_i are the stress tensor, strain tensor, the i-th component of the electric displacement, the j-th component of the electric field, elasticity tensor, piezoelectric constant tensor, permittivity tensor, mass density, and the i-th component of the mechanical displacement, respectively. Considering the electronic properties of piezoelectric semiconductors we must also take into account, the continuity equation, the Maxwell-Poisson equation and the free current density for

electrons as written in the following:

$$\begin{aligned}\frac{\partial J_i}{\partial x_i} &= -\frac{\partial \rho_e}{\partial t} = q\frac{\partial n_s}{\partial t},\\ \frac{\partial D_i}{\partial x_i} &= \rho_e = -qn_s,\\ J_i &= q\left(n_0+n_s\right)\mu_{ij}\left(E_j^0+E_j\right)+qd_{ij}\frac{\partial\left(n_0+n_s\right)}{\partial x_j},\end{aligned} \tag{2}$$

where J_i, ρ_e, q, μ_{ij}, and d_{ij} are the free current density, space charge density, elementary charge, the electron mobility, and the diffusion constant tensors, respectively. In eqs. (2) it was assumed that all acoustically generated carriers n_s are free to move, hence the total carrier density reads

$$n = n_0 + n_s, \tag{3}$$

where n_0 is the carrier density at equilibrium. The same applies for the total electric field that is composed of a constant E_j^0 and a perturbation E_j part. Both the equilibrium carrier density and electric field are assumed to be stationary. We begin by substituting the stress tensor into the equation of motion. Since k and l are interchangeable, the wave equation is expressed in the compact form via the electrostatic potential $E_k = -\frac{\partial\phi}{\partial x_k}$:

$$\rho\frac{\partial^2 u_i}{\partial t^2} = c_{ijkl}\frac{\partial^2 u_k}{\partial x_j\partial x_l} + e_{kij}\frac{\partial^2\phi}{\partial x_j\partial x_k}. \tag{4}$$

Hereafter, we take the electric displacement field from eqs. (1) and substitute it into the Maxwell-Poisson equation, again by using the potential

$$e_{ikl}\frac{\partial^2 u_k}{\partial x_i\partial x_l} - \varepsilon_{ij}\frac{\partial^2\phi}{\partial x_i\partial x_j} = -qn_s. \tag{5}$$

Finally, the free current density is substituted into the continuity equation of eqs. (2) and upon neglecting higher-ordered products one arrives at

$$\begin{aligned}\frac{1}{q}\frac{\partial J_i}{\partial x_i} = \frac{\partial n_s}{\partial t} &= -n_0\mu_{ij}\frac{\partial^2\phi}{\partial x_i\partial x_j} + \mu_{ij}E_j^0\frac{\partial n_s}{\partial x_i}\\ &\quad + d_{ij}\frac{\partial^2 n_s}{\partial x_i\partial x_j}.\end{aligned} \tag{6}$$

We consider a piezoelectric wurtzite structure of hexagonal $6mm$ symmetry in 2D. In this regard, only u_x, u_z are considered while we discard $u_y = \partial_y = 0$. Using this crystal symmetry, the stress and electric displacement fields will then be written as

$$\begin{bmatrix}T_{xx}\\T_{zz}\\T_{xz}\\D_x\\D_z\end{bmatrix} = \begin{bmatrix}c_{11}&c_{13}&0&0&e_{31}\\c_{13}&c_{33}&0&0&e_{33}\\0&0&c_{44}&e_{15}&0\\0&0&e_{15}&-\varepsilon_{11}&0\\e_{31}&e_{33}&0&0&-\varepsilon_{33}\end{bmatrix}\begin{bmatrix}S_{xx}\\S_{zz}\\2S_{xz}\\\dfrac{\partial\phi}{\partial_x}\\\dfrac{\partial\phi}{\partial_z}\end{bmatrix}. \tag{7}$$

As we depict in fig. 2, we consider the stacking direction of individual wurtzite crystal slabs to be along z. We will assume acoustic waves to be incident along this axis, which means that the electric field must be applied parallel to the sound field. In this context we take the electric field to have a component only along this respective axis, E_z, and its derivative to vanish along the remaining direction, $\partial_x E_z = 0$. The constitutive relations in eq. (7) depict how the anisotropic piezoelectric constants are derived and similarly we take the same symmetry for μ_{ij} and d_{ij}. These relations are substituted into eqs. (4)–(6), from which ultimately four equations are constructed:

$$\begin{aligned}\rho\frac{\partial^2 u_x}{\partial t^2} &= \left(c_{11}\frac{\partial^2}{\partial x^2}+c_{44}\frac{\partial^2}{\partial z^2}\right)u_x + \left(c_{13}+c_{44}\right)\frac{\partial^2 u_z}{\partial x\partial z},\\ \rho\frac{\partial^2 u_z}{\partial t^2} &= \left(c_{44}\frac{\partial^2}{\partial x^2}+c_{33}\frac{\partial^2}{\partial z^2}\right)u_z + \left(c_{13}+c_{44}\right)\frac{\partial^2 u_x}{\partial x\partial z}\\ &\quad + e_{33}\frac{\partial^2\phi}{\partial z^2},\\ \left(e_{15}+e_{31}\right)\frac{\partial^2 u_x}{\partial x\partial z} &+ \left(e_{15}\frac{\partial^2}{\partial x^2}+e_{33}\frac{\partial^2}{\partial z^2}\right)u_z\\ &\quad - \varepsilon_{33}\frac{\partial^2\phi}{\partial z^2} = -qn_s,\\ \frac{\partial n_s}{\partial t} &= -n_0\mu_{33}\frac{\partial^2\phi}{\partial z^2} + E_z^0\mu_{33}\frac{\partial n_s}{\partial z}\\ &\quad + \left(d_{11}\frac{\partial^2}{\partial x^2}+d_{33}\frac{\partial^2}{\partial z^2}\right)n_s.\end{aligned} \tag{8}$$

This system is a compact problem to solve, which could be implemented in a finite difference or element solver. An entirely 1D treatment where we take $u_x = \partial_x = 0$ enables a fully analytical treatment with rich physical insight. In this way, we end up with a longitudinal wave polarized along z. In order to arrive there, we represent the unknown fields as plane waves $\psi = \Psi e^{i(kz-\omega t)}$, where ψ represents u_z, ϕ, and n_s and Ψ represent their complex wave amplitudes, respectively. Upon substituting this Ansatz into eq. (8), we simplify the problem into a compact system of equations

$$\begin{bmatrix}c_{33}k^2-\rho\omega^2 & e_{33}k^2 & 0\\ e_{33}k^2 & -\varepsilon_{33}k^2 & -q\\ 0 & -n_0\mu_{33}k^2 & d_{33}k^2-i\beta\end{bmatrix}\begin{bmatrix}U_z\\\Phi\\N_s\end{bmatrix} = 0, \tag{9}$$

where $\beta = E_z^0\mu_{33}k+\omega$ is an acousto-electric coupling function. The zero determinant of eq. (9) gives us the dispersion relation of the problem:

$$\rho\omega^2 = k^2\left[c_{33}+\frac{e_{33}^2}{\varepsilon_{33}}\left(1+\frac{\sigma/\varepsilon_{33}}{d_{33}k^2-i\beta}\right)^{-1}\right] = k^2 c'_{33}, \tag{10}$$

where $\sigma = qn_0\mu_{33}$ is the conductivity. From eq. (10) it can immediately be seen that we are able to derive an effective stiffness c'_{33}. Furthermore, upon solving for k, also we are able to derive its imaginary part, that is, the attenuation

coefficient α as long as the piezoelectric coupling $K^2 = e_{33}^2/(c_{33}\varepsilon_{33}) \ll 1$. These equations are written in the canonical form after Hutson and White [17,18]

$$\frac{c'_{33}}{c_{33}} = 1 + K^2 \frac{\gamma + i\frac{\omega}{\omega_d}}{\gamma + i\left(\frac{\omega_c}{\omega} + \frac{\omega}{\omega_d}\right)}, \qquad \alpha = \frac{K^2}{2}\frac{\omega}{\mathrm{v_s}} \frac{\gamma\frac{\omega_c}{\omega}}{\gamma^2 + \left(\frac{\omega_c}{\omega} + \frac{\omega}{\omega_d}\right)^2}. \tag{11}$$

In eqs. (11) $\gamma = 1 - \mathrm{v_d}/\mathrm{v_s}$ is a drift parameter where the velocity $\mathrm{v_s}$ is the sound speed of the semiconductor and $\mathrm{v_d} = \mu_{33}E_z^0$ corresponds to the drift velocity. $\omega_c = \sigma/\varepsilon_{33}$ and $\omega_d = \mathrm{v_s}/d_{33}$ represent the diffusion relaxation and the diffusion frequency, respectively. These analytical expressions provide extensive insight into the acousto-electric effect under investigation. However, in order to solve the dispersion relation in eq. (10) we employ an exact model that describes the piezoelectric interaction to second-order accuracy in the mobility μ_{33} [19]. We obtain two modal solutions whose wave numbers are denoted as k_1 and k_2. These solutions correspond to one piezoelectric mode propagating with the electric flow and one that is opposite to it.

$\mathcal{PT}$ symmetry properties in zinc oxide. – In order to satisfy the condition of phononic $\mathcal{PT}$ symmetry, the mass density and the effective stiffness must fulfil the conditions $\rho(z) = \rho(-z)$ and $c'_{33}(z) = c'^{*}_{33}(-z)$, respectively [20]. These conditions demand an equal amount of loss and gain in the system, which we will investigate in the following with the aid of the expression for the damping α in eqs. (11). We begin by plotting the dependence of α with $\pm\mathrm{v_d}/\mathrm{v_s}$ in fig. 1(a) to demonstrate the transition from positive to negative attenuation in doped ZnO at 200 MHz. The electron drift obviously is controlled through the electric field whose direction is along z, the axis of sound propagation. At the Cherenkov threshold, $\mathrm{v_d}/\mathrm{v_s} = 1$, phonon amplification starts to kick in. For backward directed sound propagation $\mathrm{v_d}/\mathrm{v_s} < 0$, as seen in fig. 1(a), waves are always damped (positive attenuation). This feature has to be born in mind when designing $\mathcal{PT}$ symmetry. *E.g.*, when a finite slab is biased with an electric field, say, above the Cherenkov threshold, then sound is amplified in forward direction only. At the same field strength, as we discussed above, sound travelling in the reverse direction is always damped without a crossover towards gain. A typical binary system, one that contains a loss unit and the gain counterpart, must therefore be balanced in forward and backward sound propagation. In other words, α_{gain} is composed of bi-directional attenuation within the region of interest $1.0 \leq |\mathrm{v_d}/\mathrm{v_s}| \leq 1.20$ and equivalently for the loss component, α_{loss} within $0.8 \leq |\mathrm{v_d}/\mathrm{v_s}| \leq 1.0$ as seen in fig. 1(b). In fig. 1(b), we detune the total attenuation $\alpha_{\mathrm{gain}} + \alpha_{\mathrm{loss}}$ from a quasi-balanced state towards zero net amplification or damping $\alpha_{\mathrm{gain}} + \alpha_{\mathrm{loss}} = 0$. The quasi-balanced state refers to the Cherenkov threshold where

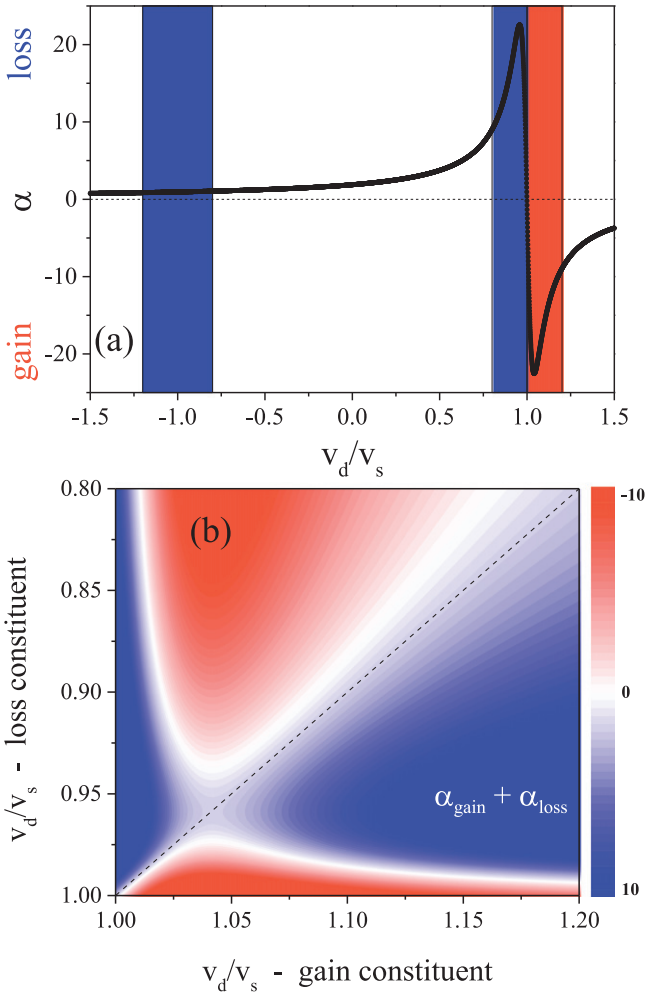

Fig. 1: (Colour online) Gain/damping of sound in unbound ZnO. The frequency is locked at 200 MHz and the carrier concentration is $n = 10^3 n_i$, where n_i is the intrinsic density. (a) Attenuation (positive and negative in 1/m) is plotted against the applied drift velocity that is expressed via the drift compared to the sound velocity. The acoustic operation of interest in forward and backward sound propagation ($\pm\mathrm{v_d}/\mathrm{v_s}$) is marked within the respective gain (red) and loss (blue) regions. (b) The sum of the total acoustic amplification α_{gain} and damping α_{loss} after a round trip is plotted around the Cherenkov threshold, $\mathrm{v_d}/\mathrm{v_s} = 1$. Symmetric detuning is indicated by the dashed line.

attenuation is exactly zero in forward direction only, see fig. 1(a), but contains some damping in the reverse direction. Increasing loss and gain steadily, gives rise to the total attenuation whose contour can be traced back to the gain/loss profile in fig. 1(a). The absence of gain for $\mathrm{v_d}/\mathrm{v_s} < 0$ shows that gain has to be increased faster in order for the total attenuation to vanish. This is shown by the slow divergence from the dashed line of symmetric detuning. However, lowering the attenuation, $\mathrm{v_d}/\mathrm{v_s} < 0.93$ broadens the tunability to balance out loss and gain.

In the following, we will implement a numerical technique to compute the complex scattering parameters of a phononic $\mathcal{PT}$-symmetric binary system. Since we have

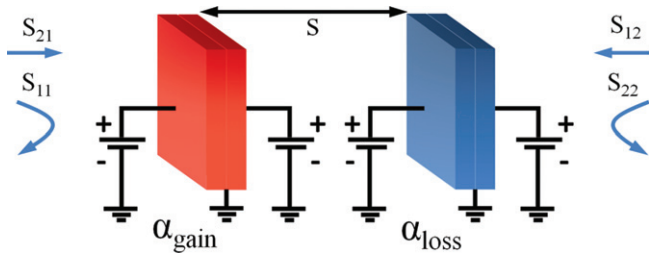

Fig. 2: (Colour online) $\mathcal{PT}$-symmetric binary system where the gain (red) and loss (blue) ZnO constituents are biased in a bi-directional fashion. The passive non-piezoelectric separator region, with $\rho = \rho^B$ and $c_{33} = c_{33}^B$, has thickness s. The scattering parameters S are shown at both the gain (with total attenuation α_{gain}) and the loss constituent, α_{loss}.

two modal solutions whose wave numbers are denoted as k_1 and k_2 the implementation is not so straightforward as compared to its optical counterpart. However, in order to illustrate the compactness of the problem we derive the scattering coefficients for a single biased slab only. Extensions to the actual problem, see fig. 2, is merely a task consisting in rigorous wave expansions for additional layers or taking the scattering coefficients for the isolated slab and introducing them into a transfer matrix that represents the entire structure. The longitudinal displacement $u(z,\omega)$ can be expanded into incoming, slab-cavity (of thickness h), and outgoing waves:

$$u(z,\omega) = \begin{cases} e^{-iqz} + S_{11}e^{iqz}, & z \leq 0, \\ \sum_{n=1}^{2} \delta_n \Phi_n e^{ik_n z}, & 0 < z < h, \\ S_{21}e^{-iq(z-h)}, & z \geq h, \end{cases} \tag{12}$$

where $q = \omega\sqrt{\rho^B/c_{33}^B}$ with ρ^B and c_{33}^B representing the background mass density and stiffness, respectively. Furthermore, S_{11}, S_{21} represent the reflection and transmission coefficient in forward direction, whereas the electric potential Φ_n is related to the displacement $u(z,\omega)$ via

$$\delta_n = -\frac{e_{33}k_n^2}{c_{33}k_n^2 - \rho\omega^2}. \tag{13}$$

When a dc field is applied, the elastic displacement will follow a stationary motion and one that varies in time. We only consider the dynamic one as it suffices for the boundary value problem. In this regard, at the interfaces of the slabs, continuity of the displacement and normal stress T_{zz} has to be imposed. This gives rise to a system of equations where the fields are matched at their respective boundaries,

$$\begin{aligned} 1 + S_{11} &= \sum_{n=1}^{2} \delta_n \Phi_n, \\ -1 + S_{11} &= \sum_{n=1}^{2} \eta_n \Phi_n, \\ S_{21} &= \sum_{n=1}^{2} \delta_n \Phi_n e^{ik_n h}, \\ S_{21} &= -\sum_{n=1}^{2} \eta_n \Phi_n e^{ik_n h}. \end{aligned} \tag{14}$$

Here

$$\eta_n = \frac{k_n}{\omega\sqrt{\rho^B c_{33}^B}}\left(\delta_n c_{33} + e_{33}\right) \tag{15}$$

relates Φ_n to the normal stress T_{zz}. In eqs. (14) we immediately find expressions for S_{11} and S_{21}, but when eliminating these coefficients, we obtain a simplified system of equations of unknown potentials Φ_n,

$$\begin{bmatrix} (\delta_1 - \eta_1) & (\delta_2 - \eta_2) \\ (\delta_1 + \eta_1)\, e^{ik_1 h} & (\delta_2 + \eta_2)\, e^{ik_2 h} \end{bmatrix} \begin{bmatrix} \Phi_1 \\ \Phi_2 \end{bmatrix} = \begin{bmatrix} 2 \\ 0 \end{bmatrix}. \tag{16}$$

Hence, upon solving for Φ_n we find the scattering coefficients. Similarly, when the direction of sound propagation is reversed by either flipping the sign of the electric field or matching the displacements in reverse order as compared to eqs. (12), we obtain the remaining scattering parameters S_{22} and S_{12}. The S parameters for a single biased piezoelectric slab read

$$\begin{aligned} S_{11} &= \frac{2}{D}\left[-\delta_2\left(\delta_1 + \eta_1\right)e^{ik_1 h} + \delta_1\left(\delta_2 + \eta_2\right)e^{ik_2 h}\right] - 1, \\ S_{21} &= \frac{2}{D}\left[-\delta_2\left(\delta_1 + \eta_1\right) + \delta_1\left(\delta_2 + \eta_2\right)\right]e^{i(k_1+k_2)h}, \\ S_{22} &= \frac{2}{D}\left[\delta_2\left(\delta_1 - \eta_1\right)e^{ik_2 h} - \delta_1\left(\delta_2 - \eta_2\right)e^{ik_1 h}\right] - 1, \\ S_{12} &= \frac{2}{D}\left[\delta_2\left(\delta_1 - \eta_1\right) - \delta_1\left(\delta_2 - \eta_2\right)\right], \end{aligned} \tag{17}$$

where $D = (\delta_1 - \eta_1)(\delta_2 + \eta_2)e^{ik_2 h} - (\delta_1 + \eta_1)(\delta_2 - \eta_2)e^{ik_1 h}$. In an equal manner, the overall scattering coefficients for the entire structure illustrated in fig. 2 can be obtained. However, as we mentioned above, this is possible only on numerical grounds due to the complexity of piezoelectric waves. Henceforth, we proceed by investigating the complex scattering characteristics of the $\mathcal{PT}$-symmetric binary system where each loss and gain component are electrically biased, see fig. 2, in a bi-directional fashion [20]. The gain and loss components are separated by a passive layer of thickness s. From the overall scattering parameters of this structure, we derive the complex eigenvalues

$$\lambda_1, \lambda_2 = \frac{S_{11} + S_{22}}{2} \pm \sqrt{\frac{\left(S_{11} - S_{22}\right)^2}{4} + T^2}, \tag{18}$$

where $S_{21} = S_{12} = T$. Upon computing the scattering parameters and the eigenvalues of the problem we compare to the contour with zero net loss or gain $\alpha_{\text{gain}} + \alpha_{\text{loss}} = 0$, as plotted in fig. 1(b). In fig. 3, we calculate two examples where the upper panels plot the imaginary part of

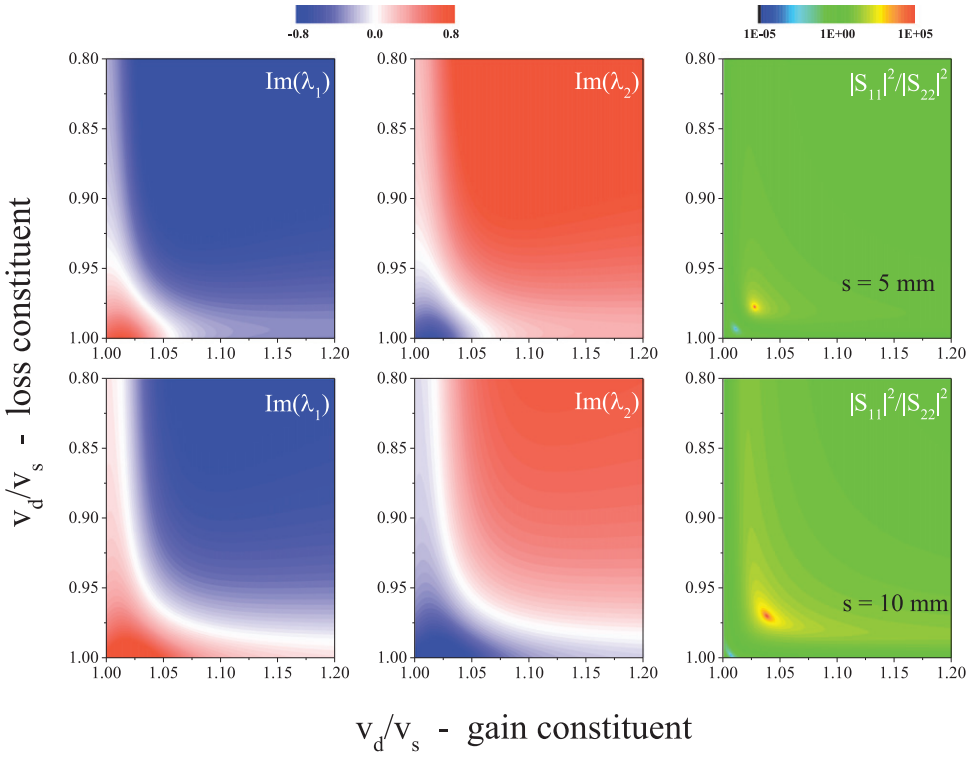

Fig. 3: (Colour online) $\mathcal{PT}$ symmetry properties around the phase transition contour. The $\mathcal{PT}$ symmetric binary system is captured in fig. 2 where the individual gain and loss slabs are 4 cm in thickness. The passive separation stub is impedance matched where two cases are studied: upper panels: $s = 5$ mm; lower panels: $s = 10$ mm. By detuning gain and loss around the Cherenkov threshold, we plot the eigenvalues λ_1, λ_2 and the rectification ratio $|S_{11}|^2/|S_{22}|^2$.

the eigenvalues $\mathrm{Im}(\lambda_{1,2})$ and the so-called rectification ratio that we measure through the reflectances $|S_{11}|^2/|S_{22}|^2$ for $s = 5$ mm, whereas the lower panels correspond to the case with $s = 10$ mm. The contour in fig. 1(b) where gain and loss are perfectly balanced illustrates where the complex eigenvalues may coalesce towards an entirely real spectrum. This is expected to occur when detuning loss and gain simultaneously beyond the quasi-balanced state. For $s = 5$ mm the coalescence of the imaginary eigenvalues takes place in a rather abrupt fashion as compared to the smooth contour for $s = 10$ mm, see fig. 3. Nonetheless, close to the symmetric line of detuning, in both cases, an exceptional point is found where the rectification ratio $|S_{11}|^2/|S_{22}|^2$ obtains maximal values. We foresee that controlling the spontaneous breaking of $\mathcal{PT}$ symmetry to be very rich since this can be accomplished in ways beyond tuning an external electric field. Taking advantage of the dispersive nature of the acousto-electric effect or modulating the attenuation through the carrier concentration makes phononic $\mathcal{PT}$ symmetry in a piezoelectric semiconductor an interesting playground for new physics.

Conclusion. – We presented a thorough theoretical framework to study phononic $\mathcal{PT}$ symmetry where loss and gain are electrically tuned in ZnO via the acousto-electric effect. By carefully biasing the loss and gain units, we explored exceptional contours at which one-way suppressed acoustic reflectance is realized. We expect great implications for unidirectional cloaks of invisibility and other possible metamaterials related applications [21].

* * *

JC gratefully acknowledges financial support from the Danish Council for Independent Research and a Sapere Aude grant (no. 12-134776). Fruitful discussions with Morten Willatzen and Ming-Hui Lu are gratefully acknowledged.

REFERENCES

[1] Bender C. M. and Boettcher S., *Phys. Rev. Lett.*, **80** (1998) 5243.
[2] Schomerus H., *Phys. Rev. Lett.*, **104** (2010) 233601.
[3] Ruter C. E., Makris K. G., El-Ganainy R., Christodoulides D. N., Segev M. and Kip D., *Nat. Phys.*, **6** (2010) 192.
[4] Lin Z., Ramezani H., Eichelkraut T., Kottos T., Cao H. and Christodoulides D. N., *Phys. Rev. Lett.*, **106** (2011) 213901.
[5] Regensburger A., Bersch C., Miri M. A., Onishchukov G., Christodoulides D. N. and Peschel U., *Nature (London)*, **488** (2012) 167.

[6] Chong Y. D., Ge L., Cao G. and Stone A. D., *Phys. Rev. Lett.*, **105** (2010) 053901.
[7] Ge L., Chong Y. D. and Stone A. D., *Phys. Rev. A*, **85** (2012) 023802.
[8] Sun Y. *et al.*, *Phys. Rev. Lett.*, **112** (2014) 143903.
[9] Peng B. *et al.*, *Nat. Phys.*, **10** (2014) 394.
[10] Longhi S., *Phys. Rev. A*, **82** (2010) 031801(R).
[11] Feng L., Wong Z. J., Ma R.-M., Wang Y. and Zhang X., *Science*, **346** (2014) 972.
[12] Hodaei H. *et al.*, *Science*, **346** (2014) 975.
[13] Schindler J., Lin Z., Lee J. M., Ramezani H., Ellis F. M. and Kottos T., *J. Phys. A*, **45** (2012) 444029.
[14] Xu X.-W., Liu Y.-X., Sun C.-P. and Li Y., *Phys. Rev. A*, **92** (2015) 013852.
[15] Fleury R., Sounas D. L. and Alu A., *Nat. Commun.*, **6** (2015) 5905.
[16] Shi C. *et al.*, *Nat. Commun.*, **7** (2016) 11110.
[17] Hutson A. R. *et al.*, *Phys. Rev. Lett.*, **7** (1961) 237.
[18] White D. L., *J. Appl. Phys.*, **33** (1962) 2547.
[19] Christensen J. and Willatzen M., *Acta Acust. united with Ac.*, **101** (2015) 986.
[20] Christensen J., Willatzen M., Velasco V. R. and Lu M.-H., *Phys. Rev. Lett.*, **116** (2016) 207601.
[21] Cummer S. A., Christensen J. and Alu A., *Nat. Rev. Mater.*, **1** (2016) 16001.